Deep-Sea Research I 105 (2015) 41–52

Contents lists available at ScienceDirect

Deep-Sea Research I

journal homepage: www.elsevier.com/locate/dsri

Mediterranean waters along and across the Strait of Gibraltar, characterization and zonal modification

Cristina Naranjo [a,*], Simone Sammartino [a], Jesús García-Lafuente [a], María J. Bellanco [b], Isabelle Taupier-Letage [c]

[a] Grupo de Oceanografía Física, Universidad de Málaga, 29071 Málaga, Spain
[b] Centro Oceanográfico de Cádiz, Instituto Español de Oceanografía (IEO), 11006 Cádiz, Spain
[c] Aix Marseille Université, CNRS, Université de Toulon, IRD, MIO UM 110, Antenne de la Seyne, 83507 La Seyne, France

ARTICLE INFO

Article history:
Received 14 March 2015
Received in revised form
25 June 2015
Accepted 12 August 2015
Available online 19 August 2015

Keywords:
Strait of Gibraltar
Mediterranean outflow
Water masses
Cluster analysis

ABSTRACT

Hydrological data collected in the Strait of Gibraltar have been used to examine the distribution and spatial–temporal evolution of the water masses in the area. The spatial variability has been addressed by means of a clustering method that determines the affinity of a collection of temperature–salinity samples to one of the water masses involved in the exchange. The method, which has been applied to a nearly-synoptic data set, highlights the clear evolution of the Mediterranean Waters as they flow westward through the Strait. While up to four different Mediterranean Waters are spatially distinguishable east of the main sill of Camarinal in the Strait, most of their differentiating characteristics are eroded after flowing over this restrictive topography due to mixing. West of the sill, therefore, speaking of a unique Mediterranean Water seems more appropriate. The same applies to the North Atlantic Central Water flowing in the opposite direction, which is noticeably modified along its path to the Mediterranean Sea, most of its transformation taking place in the Camarinal sill surroundings. A series of repeated transects carried out in the eastern and western sides of the Strait, provided a temporal analysis of the water masses evolution: the temporal variability manifests seasonality in the surface waters, while interannual signal is mainly detected in the deeper water masses. It is worth remarking the statistically significant positive trend of Western Mediterranean Deep Water (0.009 °C/year) and Winter Intermediate Water (0.03 °C/year), with the latter showing also intermittent occurrence in the Strait.

1. Introduction

In the Mediterranean Sea (MedS, hereinafter) the Atlantic Water (AW) that flows in through the Strait of Gibraltar (SoG) is modified by evaporation and transformed into Mediterranean water, saltier and denser, which ends up flowing out through the SoG to the Atlantic Ocean. A simplified Mediterranean basin is schematized by an eastern and a western basins connected by the Strait of Sicily. In the eastern basin, Levantine Intermediate Water (LIW) is formed through open-sea convection. In the western basin, more specifically in the Gulf of Lion, Western Mediterranean Deep Water (WMDW) is formed by deep convection. It was known since long ago that the LIW was a permanent contributor to the outflow. However, the possibility that the WMDW was participating significantly in the outflow was first presented by Stommel et al. (1973), who attributed its presence to the Bernouilli aspiration of this water from great depth in the MedS over the main sill of Camarinal in the SoG. Subsequently, other authors have revisited the topic and stressed this thought (Bryden and Stommel, 1982; Gascard and Richez, 1985; Whitehead, 1985; Kinder and Parrilla, 1987; Kinder and Bryden, 1990; Millot and Taupier-Letage, 2005; García Lafuente et al., 2007; Naranjo et al., 2012; Naranjo et al., 2014) At present, it is accepted that this deep water is a permanent part of the outflow.

Studies dealing with the outflow within and nearby the SoG used to focus on the two main Mediterranean Waters (MWs hereinafter), the LIW and the WMDW (Pettigrew, 1989; Bray et al., 1995; García Lafuente et al., 2007), which are easily identified by the maximum and minimum potential temperature, respectively, in the densest part of the θ–S diagram (Gascard and Richez, 1985). Recent efforts made to clarify the hydrological characteristics of the water masses leaving the MedS through the SoG have suggested the presence of other Mediterranean water masses, more specifically, the Tyrrhenian Dense Water (TDW) and the Winter Intermediate Water (WIW) (Rhein et al., 1999; Millot et al., 2006; Millot, 2009, 2014a,b). The first is formed by the mixing of old

* Corresponding author.

http://dx.doi.org/10.1016/j.dsr.2015.08.003
0967-0637/

WMDW residing in the Tyrrhenian Sea with newly entered LIW flowing into the western MedS through the Strait of Sicily (Rhein et al., 1999; Millot et al., 2006). The WIW is seasonally formed by convection of cooled modified Atlantic Water under severe winter condition along the continental shelf of the Liguro-Provençal subbasin and Catalan Sea (Conan and Millot, 1995; Vargas-Yáñez et al., 2012). At its source, it is the coolest water in the Western MedS (Salat and Font, 1987; Lopez Jurado et al., 1995; Millot, 1999) and it is easily detected in any θ–S diagram by a minimum of potential temperature between potential density anomaly σ_θ=28.0 and σ_θ=29.0 (Millot, 2014a). The volume of formed WIW has been reported to show marked interannual fluctuations (Pinot et al., 2002; Monserrat et al., 2008), the case of no formation being non-discardable (Pinot et al., 2002; Ribó et al., 2015).

These MWs are rather well differentiated (when present) at the eastern side of the SoG (Fuda et al., 2000; Millot, 2009), but the question remains as whether or not they are still distinguishable at the western part of the SoG once the Mediterranean outflow has crossed the Camarinal sill. The reason behind this noticeably different spatial distribution of the water masses in both halfs of the SoG (East–West) is the outstanding tidal dynamics in the area (Candela et al., 1990; Bryden et al., 1994; García-Lafuente et al., 2000; García Lafuente et al., 2007), which is strongly enhanced in the surrondings of Camarinal sill and westwards of it (Wesson and Gregg, 1994; Sánchez Garrido et al., 2008; Sánchez Garrido et al., 2011).The barotropic tidal currents interact with the SoG's topography, mainly with Camarinal sill, to produce a remarkable internal tide (Candela et al., 1990; Bryden et al., 1994; García-Lafuente et al., 2000) that in turn gives rise to dissipation rates that are amongst the highest found in the world ocean (Wesson and Gregg, 1994). The supercritical-to-subcritical flow transitions at the different critical (in hydraulic sense) sections, that happen not only in Camarinal sill but also oceanwards of it at specific times of the tidal cycle, drive that enhanced mixing (Sánchez Garrido et al., 2011; García Lafuente et al., 2013), which is the responsible for the fading out of the water masses identities in the western half of the SoG.

On the other hand, Millot (2014a), using schematic mixing lines in the Mediterranean zone of a θ–S diagram, has proposed that the four MWs can be still detected as far as at 6º15′ W to the West of the main sill and, even, traced along the Gulf of Cadiz in the Atlantic Ocean. This stand point differs from the widespread view of a Mediterranean Water that exits the SoG as a rather well mixed plume with typical properties of $\theta\sim$13 °C and $S\sim$38.4 (Baringer, 1993; Baringer and Price, 1997) in which the different MWs water masses are not discernable.

With the aim of provide a clear and standardized method to classify the water masses in the SoG, this work proposes a statistical method to automatically classify every water mass involved in the exchange. Two sets of data, described in Section 2, were specifically collected in the SoG area to address the topic. The first dataset was acquired during the Gibraltar International Campaign (GIC, Section 2.1) and the second one throughout the lifespan of the INGRES projects (Section 2.2) funded by the Spanish Government. Section 3 describes the data processing, paying special attention to the description of the proposed method of analysis (Section 3.2). The hydrological information contained in these two sets of data has been exploited in different ways in this study. GIC data were collected during a very short period and allow us to make a quasi-synoptic description of the water masses distribution in the SoG. On the contrary, INGRES data gather samples spanning a rather long period of time and have the potential of addressing the time variability and evolution of the water masses. Section 4 discusses both topics in Sections 4.1 (GIC) and 4.2 (INGRES) respectively. Finally, Section 5 summarizes the findings and conclusions of the study.

2. Data

2.1. CTD and MVP data from Gibraltar International Campaign

In the framework of the international Hydrochanges programme sponsored by the Commission Internationale pour l'Exploration Scientifique de la Méditerranée (Mediterranean Science Commission, CIESM) and supported by the HyMeX programme, the French *Mediterranean Institute of Oceanography* carried out the *Gibraltar International Campaign* on board the R/V Tethys II from the 4th to the 6th July 2012. The cruise was aimed at obtaining high resolution Conductivity–Temperature–Depth (CTD) profiles along the transects as shown in Fig. 1 in order to give an accurate water mass characterization and distribution of Mediterranean waters within the SoG. Except for section R5, a Moving Vessel Profiler (MVP) was employed; this instrument allows semi-autonomous sampling of the water column with very high spatial resolution (horizontal averaged resolution is 500 m while vertically resolution is 1 m). A drawback of the MVP is its limited range depth (~350 m). Transect R5 and a repetition of transect R2 were sampled with a CTD probe (SBE 911plus CTD, sampling frequency of 24 Hz) that reached the seafloor. The CTD vertical profiles in these transects, however, are substantially further apart than MVP profiles (typical distance between casts ranging from 1 to 3 Km).

2.2. Historical CTD data from INGRES project

The INGRES projects were initiated in 2004 with the objective of monitoring the Mediterranean outflow and its variability in response to subinertial and longer-term forcing as well as the hydrological properties of the densest and, hence, deepest Mediterranean water leaving the MedS. At the time of this study the monitoring, which is planned to be kept on position *sine die*, is still in progress. Whenever the station was serviced (every 4 or 6 months) and weather permitting, CTD transects were accomplished. Among them, transects labeled TES and TAC in Fig. 1 have been repeatedly sampled during the lifespan of INGRES projects. They make up an unevenly distributed time series since the meteorological conditions often prevented the accomplishment of one or both transects. Overall, TES was sampled 15 times and TAC 12 times (details about the dates when these transects were collected are shown in Table 1).

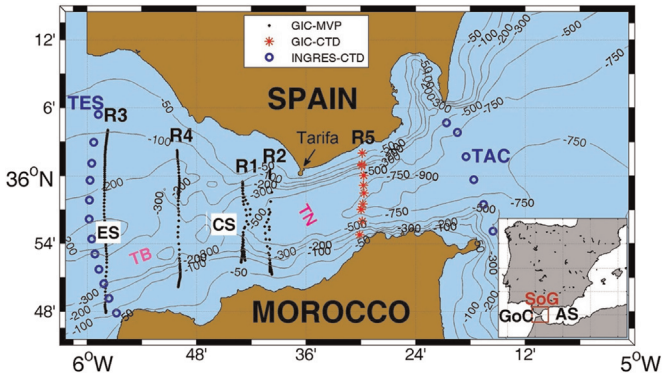

Fig. 1. Map of the Strait of Gibraltar showing bathymetric contours, in meters. The black dots and red asterisks indicate the location of the vertical profiles along the 5 sampled sections for MVP and CTD data in GIC campaign (R1–R5), respectively. Blue circles represent the two CTD sections regularly repeated in the INGRES project (TAC and TES). The main sills of Espartel (ES) and Camarinal (CS), the small Tangier Basin (TB) between them and the Tarifa Narrows (TN) are also indicated. The inset shows the location of the Strait (SoG) between the Alboran Sea (AS), the westernmost basin of the Mediterranean Sea, and the Gulf of Cadiz (GoC) in the Atlantic Ocean. (For interpretation of the references to colour in this figure legend, the reader is referred to the web version of this article.)

Table 1
Data from the INGRES project were collected unevenly spaced in time, this table summarizes the details of the dates when each transect presented in this work was carried out.

INGRES data														
TES	2005	2007	2008	2011			2012		2013		2014			
	Feb	Oct	Mar	Mar	Ago	Sep	Ago	Oct	Jun	Sep	Mar	Jun	Oct	Dec
TAC		2009	2010		2011		2012		2013		2014			
		Jun	Jul	Nov	Ago	Nov	Ago	Nov	Jun	Sep	Apr		Oct	

TAC, located at the eastern entrance of the SoG, is the last MedS transect where the MWs may be found as unmixed as in the interior of the Alboran Sea, the westernmost basin of the MedS. Further west, the enhanced turbulence associated with the tidal dynamics and the very hydrodynamics of the exchange (Wesson and Gregg, 1994; Sánchez Garrido et al., 2011) favours the mixing and erodes the specific θ–S characteristics of the different MWs participating in the outflow. The TES transect on the other hand lays along the western boundary of the SoG and represents its last gateway for the MWs before they plunge down into the Gulf of Cádiz and the Atlantic Ocean.

3. Methodology

3.1. Definition of Water masses in the Strait of Gibraltar

Beside the four MWs that can be detected in the outflow (LIW, WIW, TDW and WMDW), two AWs, the Surface Atlantic Water (SAW) and North Atlantic Central Water (NACW) shape the inflow. Therefore, a total of six water masses may be involved in the exchange. In order to provide the necessary inputs for the cluster analysis (Section 3.2), all of them have to be defined by certain hydrological characteristics that locate them in the θ–S diagram. This identification is a necessary step to quantify their influence, importance, and distribution in the SoG.

There is no general agreement about the values characterizing each water mass. Table 2 summarizes the information coming from different sources, which differs slightly from one another due to the marked spatial and time variability in the SoG. Along with this information, Table 1 shows the θ–S characteristics assigned to each of the six water masses in this study. These reference values have been selected specifically for the data set analysed in this work, after the observation of the θ–S diagram of the whole GIC and INGRES casts (Fig. 2). Despite being inside the range mentioned in the literature, the chosen values are subjective. However, the important issue for our study is to maintain unaltered these values when analysing the different CTD transects in order to have the outputs of the analysis comparable.

The noticeable seasonality of the SAW (Bray et al., 1995) caused by the heat exchange with the atmosphere coerced us to define two different θ values for this water mass, depending on when the measurements were collected (see Table 1). In summer months, the potential temperature representing this water was set to 19.7 °C. If the maximum temperature found in the sampling exceeded 19.7 °C, this maximum replaced the $\theta = 19.7$ °C reported in Table 1.

3.2. Classification of the water masses: cluster analysis

3.2.1. The cluster analysis

The cluster analysis is a mathematical tool used in this work to assess the presence and prevalence of each of the water masses in the different transects sampled in GIC and INGRES datasets. The cluster analysis is a multivariate method that aims at classifying samples on the basis of a set of measured variables. The method

Table 2
Historical values of the hydrological characteristics of the six water masses involved in the exchange through the SoG. Italicized rows highlight the pair of values used in this work.

Water mass	Author	θ (°C)	Salinity (PSU)
SAW	Bray et al. (1995)	15.9–22.7	36.2–36.5
	Criado-Aldeanueva et al. (2006)	16	36.4
	GIC&INGRES March to June	*17*	*36.3*
	July to November	*19.7*	*36.3*
NACW	Bray et al. (1995)	12.7–13.3	35.7–35.8
	Criado-Aldeanueva et al. (2006)	11–17	35.6–36.5
	GIC&INGRES	*13.5*	*35.75*
LIW	Smith et al. (2008)	> 13.2	38.45–38.75
	Font (1987)	13.3	38.5
	Parrilla and Kinder (1987)	13.15–13.25	38.47–38.51
	Millot (1999)	13.2–14.0	38.5–38.7
	J. García Lafuente et al. (2007)	13.22	38.56
	GIC&INGRES	*13.23*	*38.50*
WMDW	Bray et al. (1995)	12.8–12.9	38.4–38.5
	Salat and Font (1987)	12.75–12.9	38.4–38.48
	Parrilla et al. (1986)	13.15–13.25	38.47–38.51
	Fuda et al. (2000)	12.70–13.03	38.40–38.50
	J. García Lafuente et al. (2007)	12.80	38.45
	GIC&INGRES	*12.90*	*38.48*
WIW	Vargas-Yáñez et al. (2002)	12.5 – 13.0	38.1–38.3
	Smith et al. (2008)	12.821	37.9–38.1
	Salat and Font (1987)	12.5–13.0	38.1–38.3
	Ben Ismail et al. (2014)	< 13.8	39.9–38.2
	Ribó et al. (2015)	12.7	38.1
	GIC&INGRES	*13*	*38.3*
TDW	Millot (2009)	13.0–13.1	38.48–38.51
	Santinelli et al. (2008)	12.8–13.1	38.44–38.58
	GIC&INGRES	*13.06*	*38.52*

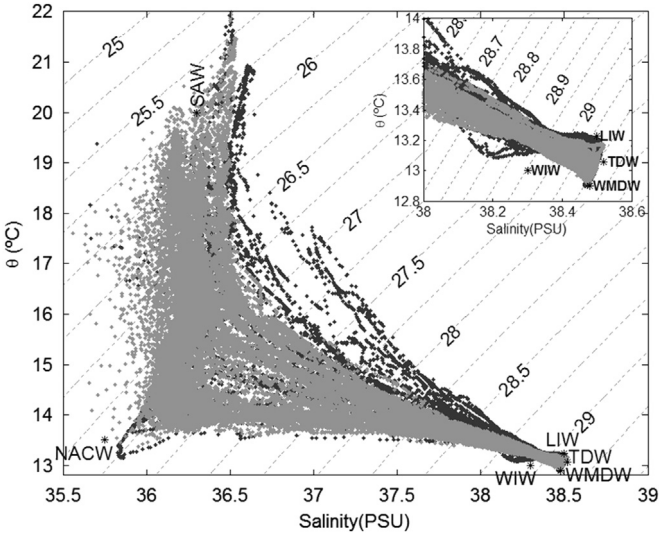

Fig. 2. θ–S diagram of the whole data set (*GIC* data in grey, *INGRES* data in black). The locations of the water masses defined by the thermohaline properties showed in Table 1 are marked by stars, with their acronyms aside. The inset is a zoom of the Mediterranean Water zone of the diagram.

separates the dataset into groups, called clusters, each cluster including samples that are more similar to each other than to the items located into another cluster, according to a given criterion.

After an initial classification of the samples (a first guess, defined by the user in the present case), the inter-cluster and intra-cluster variance is calculated, and a new distribution of the samples is proposed, which has to maximize (minimize) a certain metric that define the similarity (dissimilarity) within (between) the clusters. The algorithm iterates until it converges. The technique has been widely used to classify hydrographical datasets (Kim et al., 1991; Hur et al., 1999; Warn-Varnas et al., 2005). Classical clustering tends to give clusters with similar shape (Yan, 2005) and the method is especially appropriate to discriminate water masses with similar salinity and temperature variance. Unfortunately, this is not the case in the SoG, where MWs range much more in temperature than in salinity and AWs are largely variable in temperature, as was already remarked regarding the SAW. This drawback has been overcome by including the potential density anomaly (σ_θ) in the hydrological properties of each water mass, which is computed directly from the sea water state equation. The addition of this new variable makes the model more robust, since a water particle with the same θ–S distance to the centroid of two clusters will finally be linked to the one with more similar σ_θ, which is of concern for the isopycnal mixing taking place between the different MWs whose densities are almost the same. This inclusion hardly affects the prevailing diapycnal mixing between MWs and the overlying AWs.

Italicized rows in Table 2 and symbols in Fig. 2 give the θ–S pairs for each of the six defined water masses, which are the centroids of the clusters. While NACW, LIW, WMDW, WIW and TDW have fixed θ–S and, hence, σ_θ values, the θ of the SAW changes depending on the time of the year. Another remark concerns the WIW: due to its intermittency, this water mass may or may not be detected in the SoG. For instance and according to the zoom in the inset of Fig. 2, no traces of WIW were detected during the GIC campaign since the θ–S dots do not deviate towards the WIW centroid. In these cases, WIW must not be included in the cluster analysis. Thus, previously to carry out the analysis, each CTD cast is carefully inspected to detect the WIW and in case that a convincing evidence of its presence is not found, this water mass is excluded from the analysis of the cast in order to avoid the distortion of the results.

The metric employed to calculate the similarity between the observation and the cluster is the squared Euclidean distance

$$D_{o,c} = \sum_{i=1}^{n} \left(\vec{P_n}(i) - \vec{P_c}(i) \right)^2 \quad (1)$$

$$P_n(i) = \frac{P_o(i) - \bar{P_o}(i)}{P_{max}(i) - P_{min}(i)} \quad (2)$$

where $D_{o,c}$ is the distance between a sample at a given longitude, latitude and depth, denoted by the vector $\vec{P_n}(\theta, S, \sigma_\theta)$, and a cluster centroid, denoted by the vector $\vec{P_c}(\theta_c, S_c, \sigma_{\theta c})$, which represents a certain water mass. The θ–S–σ_θ variables and the cluster centroid have been previously normalized following (2). Sub-index "o" denotes the observed value, while "n" designate the normalized variable. "P_{max}" and "P_{min}" are the maximum and minimum observed value of the i variable. Index i stands for the i-th variable of the sample (or cluster vector), thus $n = 3$ in Eq. (1).

The fraction of a given water mass in a given sample , F_{o,c_j}, is determined by

$$F_{o,c_j} = \frac{D_{o,c_j}^{-1}}{\sum_{j=1}^{m} D_{o,c_j}^{-1}} \quad (3)$$

Table 3
Sensitivity analysis of the clustering algorithm when the θ assigned to the LIW centroid is slightly changed. The variation of θ corresponds to 20% of the difference between θ_{LIW} and the nearest water mass to LIW, θ_{TDW}. The first column shows the variation of LIW temperature over its assigned value of θ=13.23 ºC. The second column shows the percentage of samples that changed membership from one cluster to another. Columns third to seventh specify the implied clusters in the new distribution. The sum of these four columns has to coincide with column two.

$\Delta\theta_{LIW}$	Samples modified (%)	WMDW to LIW (%)	TDW to LIW (%)	LIW to TDW (%)	LIW to WMDW (%)	NACW to LIW (%)
−0.034	4.77	2.14	2.63	0	0	0
−0.019	2.44	1.44	1	0	0	0
−0.004	0.64	0.46	0.18	0	0	0
+0.011	1.40	0	0	0.37	1	0.03
+0.026	2.17	0	0	0.46	1.68	0.03

using the distance D_{o,c_j} of the sample to the centroid of cluster j ($j = 1, \cdots, m$). Distances have been normalized ($\sum_{j=1}^{m} D_{o,c_j}=1$) to have all them lying between 0 and 1. Index m is the number of cluster in the analysis, which can be 6 or 5 depending on whether or not WIW is included.

3.2.2. Sensitivity of the method

As long as the method to classify the samples in clusters depends on the cluster centroids, and so, on the definition of the water masses, its sensitivity must be tested. This will be achieved by computing the percentage of samples (measurements) that change from one cluster to another when the centroid is slightly modified.

Table 3 shows the sensitivity analysis for transect R2 (see Fig. 1) when the θ of the LIW was modified between 13.196 and 13.264 ºC, a 20% of the maximum difference for the TDW potential temperature, which is its nearest water mass.

The number of samples that were removed from their initial cluster does not reach the 5% in the worst case, which corresponds to θ_{LIW} decreasing by 0.034 ºC (first row in Table 2). In this case, LIW cluster increases at the expense of WMDW and TDW, thus removing samples near equally. On the contrary, when θ_{LIW} is raised from its chosen reference, nearly all samples leaving LIW go to WMDW cluster while a smaller proportion moves toward the TDW cluster, and a negligible portion moves from NACW to LIW. Overall, Table 3 supports the robustness of the method, as no significant changes occur if the centroids are moved within a realistic range. Similar tests have been carried out by moving other centroids with the same results.

Regardless of the accuracy of the θ–S pairs defining each cluster centroid and as long as the paper is comparing data collected in the same region with the aim of investigating the spatial-temporal variability of the water masses, the key issue is to maintain the same centroids throughout the analysis. Even when the exact proportions of the involved water masses depend slightly on the centroids choice, their relative variations from place to place and/or from time to time will be representative of the investigated variability.

4. Results

4.1. GIC dataset

The tidal variability in the SoG, subdued by semidiurnal frequencies, makes the water masses pattern be dependent on the time of the tidal cycle when the transect was accomplished (García Lafuente et al., 2007) and the tidal phase during which the sampling was carried out must be specified for each transect. This

information is provided by the sea level oscillation in Tarifa (see Fig. 1). In this regard, it is interesting to remind that the barotropic semidiurnal tide in the SoG behaves like a standing wave (García-Lafuente et al., 2000; García Lafuente et al., 2007) and that the tidal flow goes westwards during the rising tide (low to high water, or flood tide) and eastwards during the falling tide (high to low water, or ebb tide). On the other hand, the GIC sampling was accomplished during a relatively short period of time (4–6th of July, 2012). In some sense, the observations are synoptic for lower frequency fluctuations (subinertial or seasonal/interannual variability) and they should reflect the water mass composition in the SoG during that period of time, despite the tidal variability.

The results of the analysis of the GIC transects are presented from east to west in Figs. 3 and 4. During this survey, no traces of WIW were observed and the cluster analysis identifies only five water masses: WMDW, TDW, LIW, NACW and SAW.

Fig. 3 corresponds to the easternmost transect, R5, where the less mixed MWs that enter the SoG from the MedS are expected to be found. The transect was carried out from south to north with a CTD probe during the ebb tide, the last station being completed shortly after the slack tide of low water (Fig. 3a). The θ–S values of the densest water sample were 12.92–38.48 °C, which corresponds to WMDW (Fig. 3c). Fig. 3d shows that this water stacks up in the south while the LIW layer is thicker in the north, a spatial pattern that agrees with Parrilla et al. (1986) and Naranjo et al. (2012). Millot (2014b) pointed out that LIW (and also TDW to some extent) flows counterclockwise and is pushed to the north due to the Coriolis force, while the WMDW is compelled to flow attached to the southern shore preferably, where the incoming AWs, NACW in particular, are accumulated due to the Coriolis effect (Fig. 3d). Such a distribution facilitates the mixing of WMDW with AWs in the south part, a fact reflected by the mixing lines of the southernmost stations of the transect, which head directly towards the AWs region from the vicinity of the WMDW centroid (Fig. 3c). This is not so for the sations located further north in the transect where the mixing lines bend towards the LIW centroid before heading towards the AWs, showing that it is mainly the LIW and not the WMDW nor the TDW that mixes with the AWs.

The remaining transects discussed below were sampled with the MVP. The way the instrument samples the water column results in shorter times to complete a transect and higher spatial resolution (Fig. 4). However, the maximum sampled depth is less than the one reached by CTD.

Next transect to the west is R2 (panels in column I of Fig. 4). It is located to the east of CS so that the water masses have not been exposed yet to the strong mixing happening in the sill area (Wesson and Gregg, 1994; Sánchez Garrido et al., 2011). Moreover, it is not far from R5 and no significant differences are thus expected. That is the case for AWs, which depict a similar pattern (Fig. 4-I-d). However, R2 transect was sampled during the rising tide and near the high tide (Fig. 4-I-a). At this moment of the tide, the WMDW and TDW are allowed to reach shallower depths due to the interface rising associated with the internal tide (Bryden et al., 1994; Sánchez Román et al., 2012). The situation is just the opposite of R5 sampling. The most interesting feature, however, is the spatial differentiation of the MWs (Fig. 4-I-c,d) with WMDW occupying the southern part and TDW and LIW the northern area, although the latter is found at intermediate depths all over the transect.

The following transect R1 is still east, although near, of CS (R1, Fig. 4-II). It is also close to R2 so a certain similarity between them

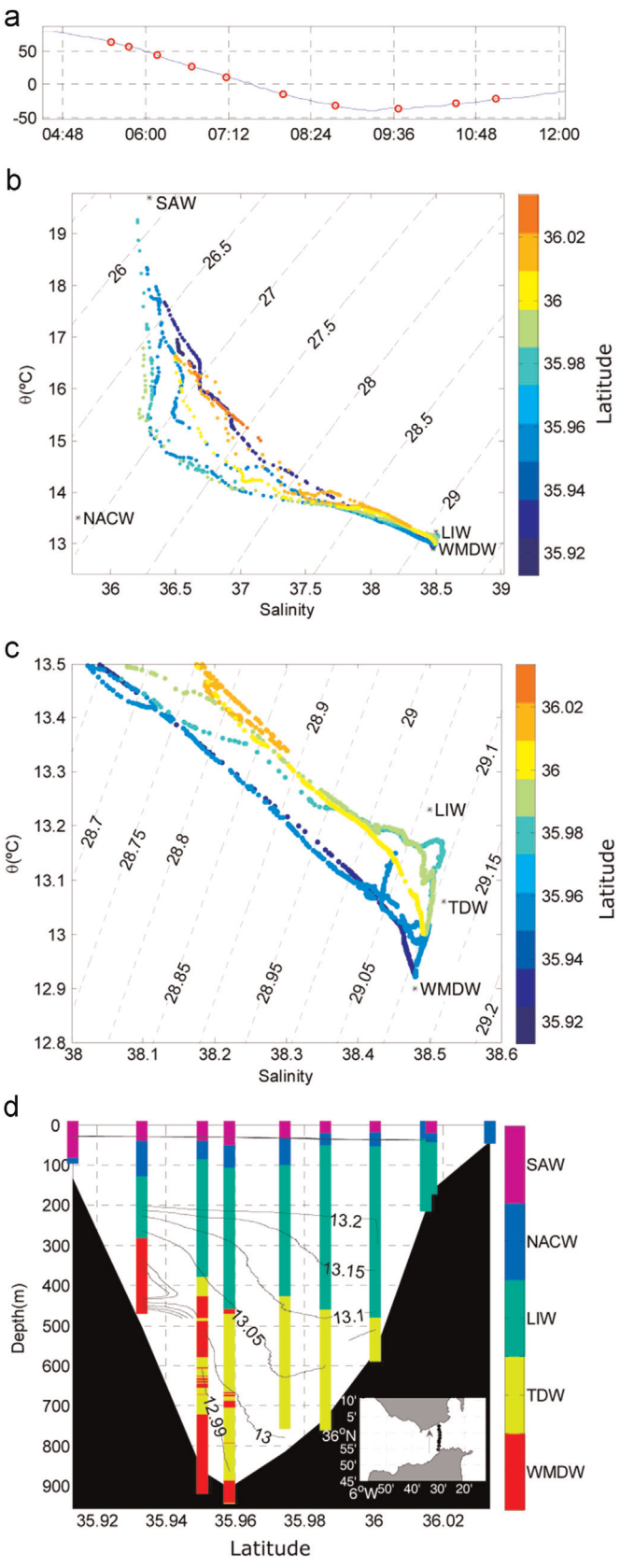

Fig. 3. (a) Tidal oscillation at Tarifa displaying the time of the CTD casts (red dots) in the R5 transect, which was accomplished from south to north. (b) θ–S diagram showing the CTD data of the R5 transect, contours lines indicate potential density anomaly. The centroids of the different water masses are marked with asterisks and the colour scale on the right identify the different casts by their latitude. (c) Zoom of the MWs area of the θ–S diagram. (d) Results of the cluster analysis where each colour represents the cluster associated with a water mass according to the legend on the right. (For interpretation of the references to colour in this figure legend, the reader is referred to the web version of this article.)

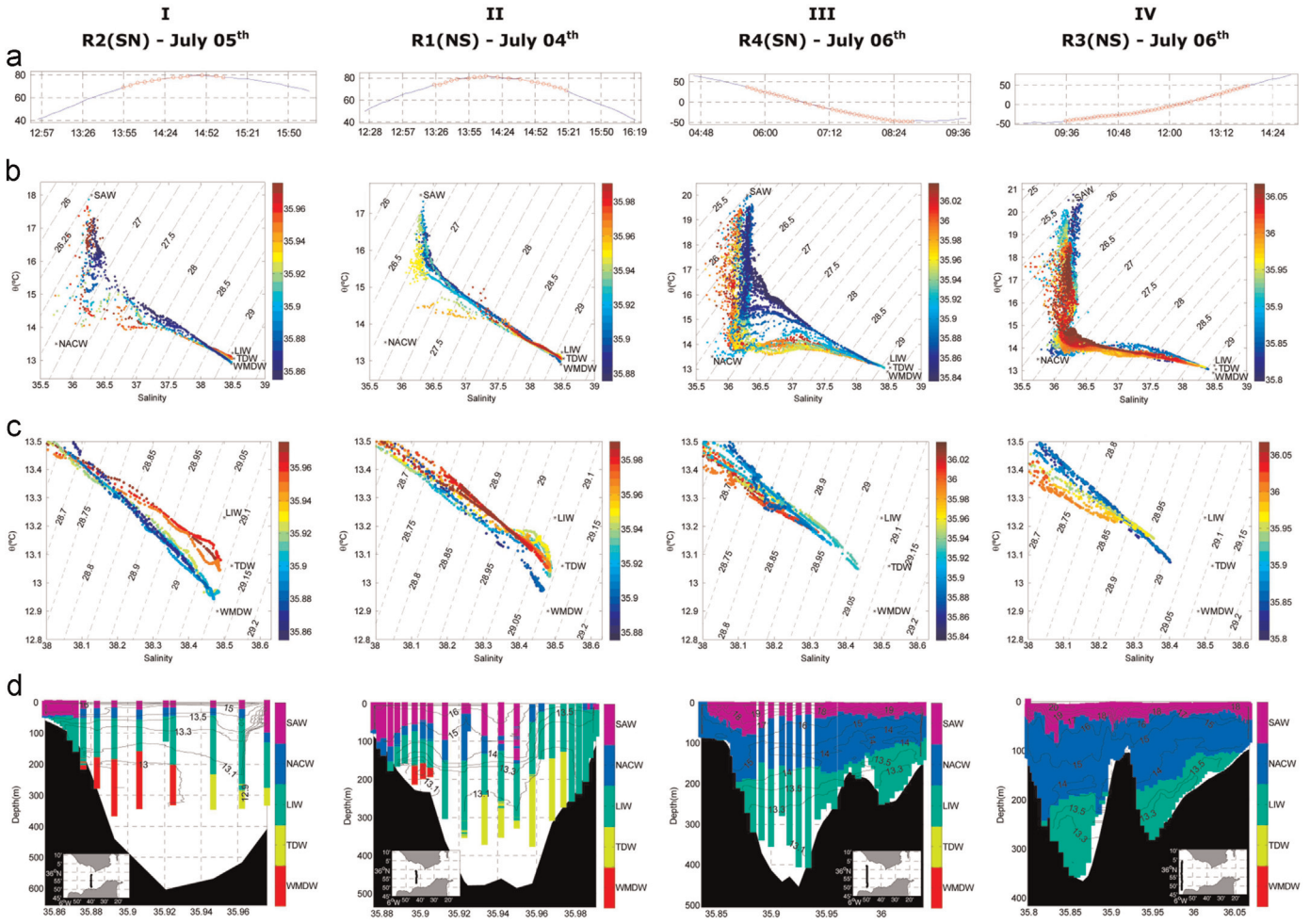

Fig. 4. Zonal evolution, from East to West, of the thermohaline properties for the different water masses involved in the exchange at the SoG. The figure is divided in four columns named I, II, III and IV and each of them is subdivided in rows. The upper row, (a), shows the sea level during the sampling of each transect, with the red circles indicating the time of the different casts. The second row, (b), displays the θ–S diagram of the whole section. The names and locations of the defined water masses are indicated, colorbar indicate latitude. The third row, (c), is a zoom of the θ–S diagram that focuses on the MWs, contours lines are σ_θ. Finally, the last row, (d), shows the classification of the water masses in the section provided by the cluster analysis. (For interpretation of the references to colour in this figure legend, the reader is referred to the web version of this article.)

is expected. But differences are apparent in the south due to the inversion of the tidal flow. R2 was accomplished from south to north and the southern stations were sampled ~1 h before the high tide during the flood tide (Fig. 4-I-a), while R1 was accomplished from north to south with the stations in the south done during the ebb tide, ~1 h after the high tide (Fig. 4-II-a). During the ebb phase the interface between AWs and MWs sinks nearby CS (Sánchez Román et al., 2008), giving rise to a considerably thicker AWs layer (Fig. 4-II-d). The northern half of both sections were sampled under similar tidal conditions near the high water, when the interface is at its shallowest position (Sánchez Román et al., 2012), and show similar accumulation of LIW and TDW and a very thin layer of AWs. The spatial differentiation showed in Fig. 4-I-c for R2 is easily recognizable in Fig. 4-II-c for transect R1 as well, which is another remarkable similarity.

Next transect to the west is R4 (Fig. 4-III), which is already west of CS. The θ–S diagram shows two noticeable differences with regard to the three previous transects. Firstly, the θ–S curves bend towards the NACW centroid, implying a much greater impact of this water mass that now spreads downwards to 200 m depth in the south (Fig. 4-III-d). Secondly, the spatial differentiation of the MWs has disappeared and now they nearly lay along a single mixing line. This is an obvious outcome of the strong mixing in the Tangier basin (Sánchez Garrido et al., 2011) which makes the MWs lose their specific identity to a great extent. The cluster algorithm only returns one kind of MWs in this transect, LIW in this case, which is somewhat misleading in view of the θ–S diagram in Fig. 4-III-c. Therefore, it requires clarification. The algorithm situates the water samples in a cluster, which is the one with the greater percentage of the water mass defined by the corresponding centroid. According to the chosen metrics (Eq. (1) and (2)), the deep water samples in this transect (and also in the next one, R3, commented below) have similar proportions of the three MWs but a slightly higher proportion of LIW (Fig. 5[1]). Should we have displaced any of the centroids of the MWs by a tiny distance, the algorithm would have possibly returned a different prevailing cluster. The reasonable conclusion is that the MWs are hardly distinguishable once the Mediterranean outflow has passed CS and that the sensible option is to speak of a unique "Mediterranean water".

On the other hand, it is noteworthy here the effect of adding σ_θ to the metrics. Should it not be included, all the deep water would have been classified as TDW with an overwhelming percentage, as

[1] Figures like Fig. 5 are helpful in order to supplement the information displayed in figures like Figs. 4 or 7. However, and in order to keep the length of the manuscript within a reasonable limit, such Figures are not included in the text, but they are offered as supplementary material.

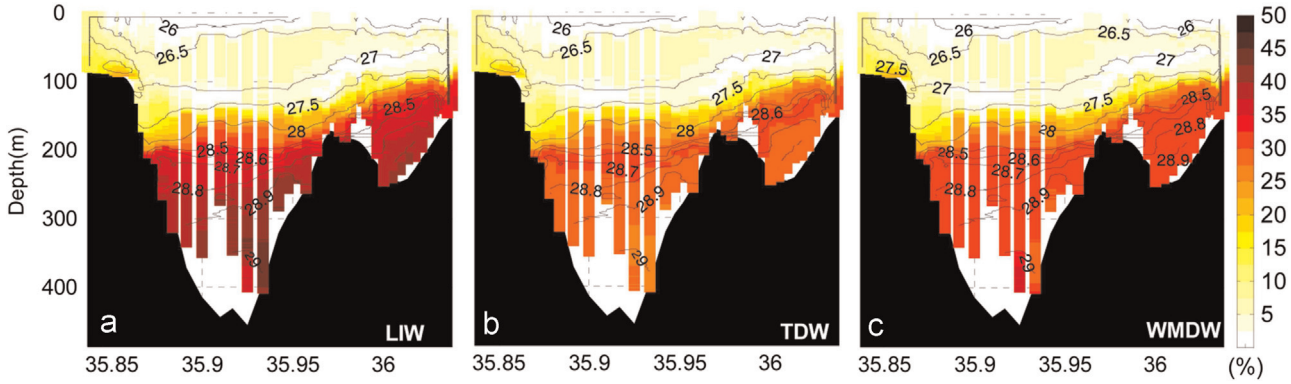

Fig. 5. Percentage of the MWs in transect R4 (Fig. 4, column III). The sum of the three contributions gives the 100% in the Mediterranean layer. The colour scales go from 0 to 50% for the sake of clarity. Contours represent the σ_θ. (For interpretation of the references to colour in this figure legend, the reader is referred to the web version of this article.)

can be easily deduced from Fig. 4-III-c. Its inclusion in the metrics makes the algorithm work more realistically in the sense that the actual sampled water is more likely to be the result of local mixing between LIW and WMDW (and TDW as well) than the outcome of the individual contribution of TDW.

The westernmost section R3, located in the western exit of the SoG, shows large similarity with the previous one. The fading out of the spatial differentiation of the MWs already detected in R4 is now more evident (Fig. 4-IV-c), and so it is the prevalence of the NACW in the Atlantic layer (Fig. 4-IV-d). Mixing lines are organized along two well-depicted directions, from MWs to NACW, and from NACW to SAW (Fig. 4-IV-b), indicating that direct mixing of MWs with SAW does not happen any longer. Notice that this mixing can be partially detected in the previous transect R4 (Fig. 4-III-b), this feature being almost the only difference among the two westernmost transects. The commentaries about the outputs of the cluster algorithm regarding the MWs made for R4 still apply in this transect.

The previous discussion has focussed on the spatial evolution of the different water masses as they flow through the SoG. Table 4 presents the θ–S values of the coldest water sampled in every transect, which is taken as a proxi of the MWs, in order to illustrate their transformation along its path to the Atlantic Ocean. To this regard, two remarks are noteworthy. The first one is about the density of the MWs: all the coldest samples are the densest samples too, except for section R1 where the densest sample has σ_θ=29.090 while the coldest sample has σ_θ=29.087 (see also Fig. 4-IIc). The second and more important remark is that the MVP does not reach the bottom so that the values reported in Table 4 should not be identified with the coldest/densest water in the section, which might not have been sampled. Even so, the regular east–west spatial trend of temperature is quite suggestive of the erosion the MWs undergo along the SoG. Table 4 also displays the coldest sample with salinity lower than 36.5, which is the best example representing NACW at each transect, in order to show the alteration of this water in its way towards the MedS. None of the former concerns apply to this water mass which has been correctly sampled by the MVP.

Table 4
The two first rows show the potential temperature and salinity, respectively, of the coldest MW sample observed in the transect (MWs block). Third and fourth rows show the potential temperature and salinity of the coldest sample with salinity less than 36.5 (NACW block). The different columns correspond to the different transects, which have been organized from east (R5) to west (R3), see Fig. 1 for details.

		R5(east)	R2	R1	R4	R3(west)
MWs	θ (ºC)	12.92	12.94	12.97	13.05	13.07
	S (psu)	38.48	38.47	38.46	38.43	38.40
NACW	θ (ºC)	14.72	14.03	14.45	13.37	13.64
	S (psu)	36.48	36.15	36.24	35.95	36.03

In the case of the MWs, θ increases and S decreases towards the west, the greatest jumps occurring between the transects R1 and R4 that surround CS, thus stressing the importance of this area as a source of turbulence (Wesson and Gregg, 1994; Sánchez Garrido et al., 2011). The same applies to the North Atlantic Central Water flowing in the opposite direction, since both θ and S tend to increase as the water flows eastward. Once again the main changes happen in the surroundings of CS, although the rising of θ and, in particular, of S still continues from R2 to R5.

4.2. INGRES

Transects TES and TAC (see Fig. 1) have been sampled repeatedly since 2004 and they are more regularly accomplished since 2011. Fig. 6 presents the θ–S diagrams of both transects confirming the already mentioned evolution of the water masses as they progress through the SoG: the fading of the spatial differentiation between MWs from TAC (east) to TES (west) and the erosion of the NACW signal from TES (west) to TAC (east). In particular, the reddish colours in the inset of Fig. 6b illustrates the fact that LIW, WIW and TDW flow preferably across the northern half of the SoG while the WMDW flows attached to the southern slope. The inset of Fig. 6a shows how the former pattern is lost at TES.

4.2.1. Spatial distribution

Fig. 7a,b show the mean potential temperature and salinity distributions at TES and TAC sections, respectively, which have been obtained by averaging all the transects collected within INGRES. Fig. 7c,d show the results of applying the cluster analysis to the same sets of data.

The cluster analysis at TAC transect shows the averaged spatial distribution of the six water masses involved in the exchange (Fig. 7d). Contrary to GIC, INGRES data recorded WIW, which now is identified flowing attached to the north shore just below a very thin layer of NACW. The remaining MWs display the same spatial pattern as in GIC: the WMDW, easily identified by $\theta < 13$ °C in Fig. 7d, resides in the deepest layer and preferably stacked up in the southern half of the transect; the TDW and LIW, which appear as a salty wedge encircled by the isohaline 38.485 (grey line in Fig. 7b), occupy an intermediate layer that thickens to the north. Any of these MWs is saltier ($S > 38.4$, see Fig. 7b) than the rather mixed MW at TES (Fig. 7a), a result that can only be explained by the entrainment of AW by the Mediterranean outflow west of Camarinal Sill, as discussed in García Lafuente et al. (2011). The

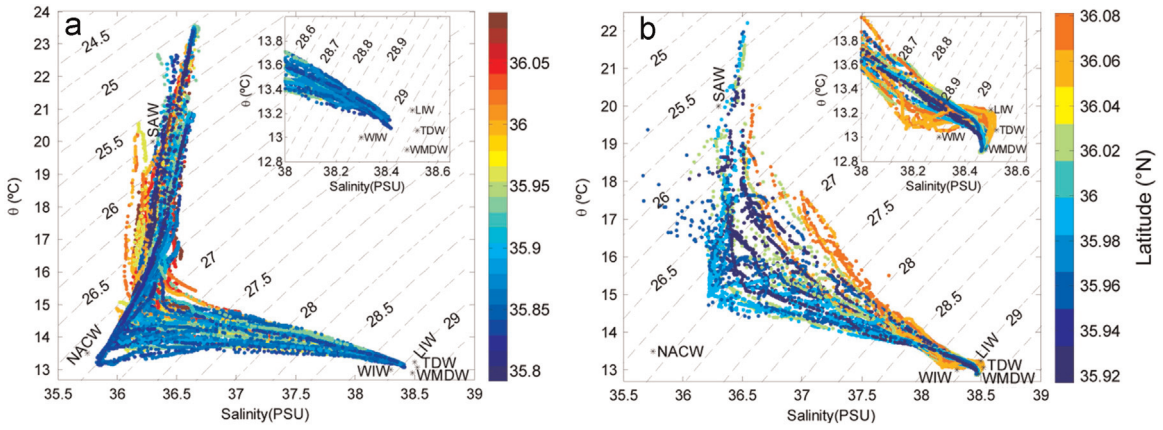

Fig. 6. θ–S diagram showing the CTD data collected at TES (a) and TAC (b) transects during the INGRES project from 2004 up to the present. The colour scale indicates latitude and the contour lines shows σ_θ . Black stars mark the θ–S pairs of the water masses involved in the exchange (see Table 2). The insets zoom in the Mediterranean water zone of the diagram. (For interpretation of the references to colour in this figure legend, the reader is referred to the web version of this article.)

two AWs are at the top of the water column in a layer that thickens from ~100 m in the north to ~150 m in the south. The presence of NACW is appreciably reduced as it experiences a marked mixing with respect to the TES transect (compare Fig. 7c and Fig. 7d). The blue colour identifying NACW in Fig. 7d must be then interpreted as the sample being closer to NACW than to any other water mass and not as if it were aside the point marking the pure NACW.

At TES, the cluster analysis only detects three water masses (Fig. 7c), in agreement with the results obtained from the GIC data in this area. The bottom layer is occupied by the MWs, which the cluster analysis identifies as LIW (the same cautionary comments on the identification of MWs as LIW made for R4 transect in the previous Section apply here). These MWs, whose averaged salinity is ~38.2 with maxima of 38.4, flow mainly through the southern channel below 250 m, the volume flowing through the northern channel being much smaller. NACW is the prevailing water mass, occupying a layer from 50 to 250 m in the southern channel (Fig. 7c). Obviously not all this layer is NACW. It includes its mixture with the overlying (SAW) and underlying (LIW) waters, with the NACW entering in greater proportion than the others. Actually, Fig. 7a shows a core of minimum salinity around 150–200 m depth in the southern channel, which would be the depth where the purest NACW is flowing.

4.2.2. Temporal fluctuations in the core of the water masses

This section addresses the time variability of the thermohaline characteristics found in INGRES data. To this aim, we have selected representative samples of each water mass with the same criterion for a given transect, although the criterion may change slightly from the west (TES) to the east (TAC) transect, as explained below.

At TAC the criterion to define each water mass must be selected carefully, as the four MWs detected in this transect have only very small thermohaline differences. The SAW is selected as the warmest sample. The most appropriate criterion for the NACW will be to take the freshest sample, but NACW has been widely altered by mixing and the freshest water criterion may be not

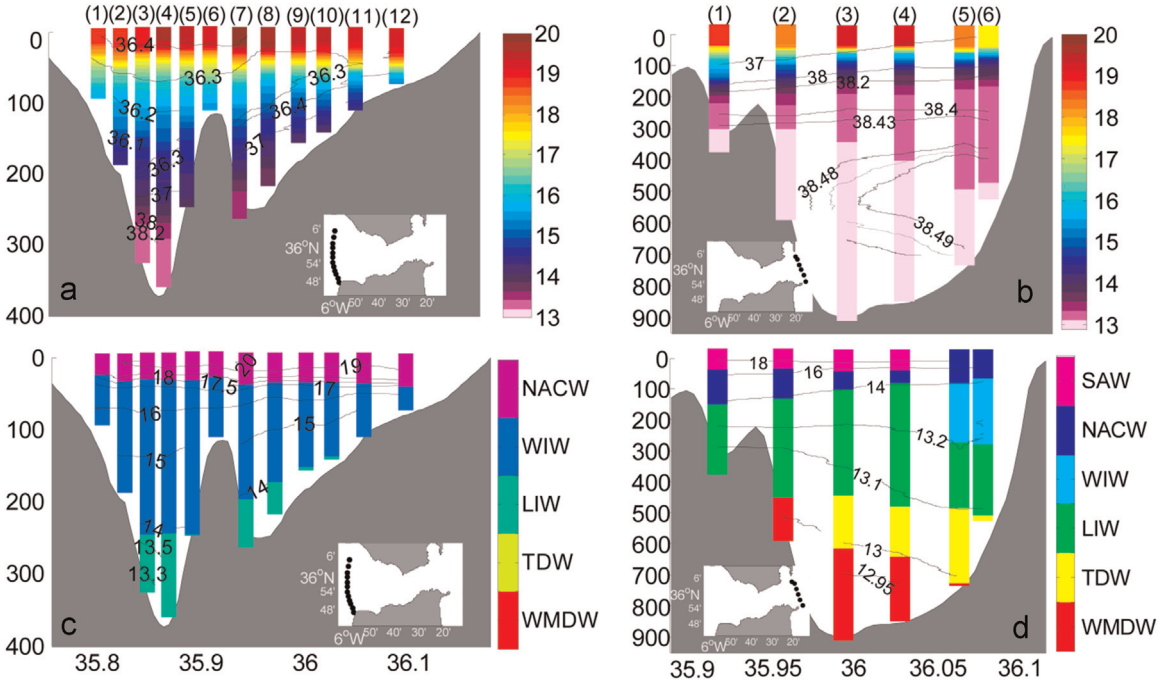

Fig. 7. Averaged potential temperature (colour scale) and salinity (labelled contours) of the whole dataset collected at TES (a) and TAC (b). Panels (c) and (d) show the distribution of water masses in these transects provided by the cluster analysis. Contours display the potential temperature. Insets show the location of the cast in each transect. (For interpretation of the references to colour in this figure legend, the reader is referred to the web version of this article.)

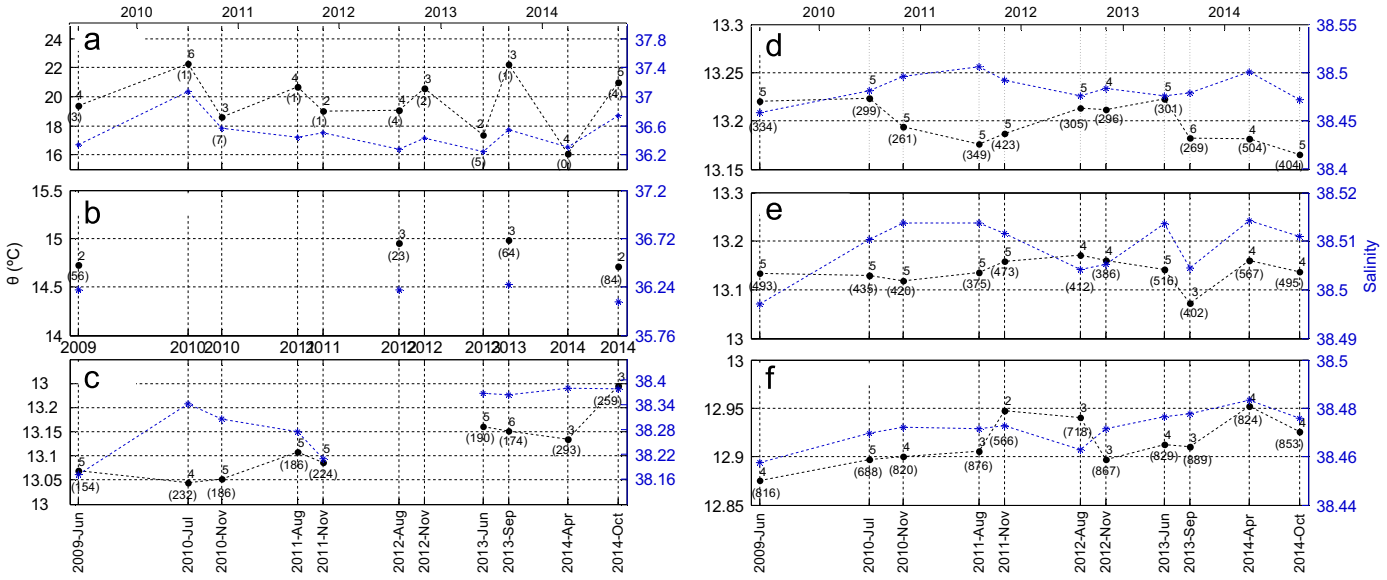

Fig. 8. Potential temperature (left axes, black dots) and salinity (right axes, blue asterisks) of the water samples representing each water masses at the TAC transect (see text for details). Numbers 1–6 aside the symbols indicate the cast were the samples were detected, according to the labels on top of Fig. 7. Numbers within brackets display the depth of the sample (in meters from the surface). Ticks in the *x*-axes at the top of the figures indicate January the 1st of each year. (For interpretation of the references to colour in this figure legend, the reader is referred to the web version of this article.)

applicable at TAC (which however is pretty suitable in the TES section, see θ–S diagram of Fig. 6b). Even more, the mixing could have been so important that speaking of NACW makes no clear sense. Thus, we only admit the presence of NACW if a clear minimum of salinity with respect to the overlying SAW is observed in the vertical profile, otherwise we ignore this water mass, even if temperature/salinity dots in the θ–S diagram bend gently towards the mark representing the NACW. Regarding the MWs, WMDW is determined as the coldest sample, TDW as the saltiest one, and LIW as the warmest whenever its salinity exceeds 38.4. As for the WIW, it is identified as the coldest sample between σ_θ=28.0 and σ_θ=29.0 (Millot, 2014a), provided that it is visually detected in the θ–S diagram previously (that is, whenever the relative minimum around the WIW position in the diagram is positively identified, see inset in Fig. 6b).

Fig. 8 shows the series of these representative samples at TAC transect, which are displayed along with the depth where the sample was found (in brackets) and the location of the profile (see labels on top of Fig. 7). The seasonality of SAW is recognizable at TAC despite being more intense in the TES section (compare Figs. 8a with 9a). As for the NACW, it was positively identified only 4 out of 11 times (Fig. 8b). In all these occasions its core mass was always found in the southern casts (cast 2 or 3) at depths between 20 and 85 m, quite shallower than at TES, where the NACW core was between 150 and 200 m (Fig. 7a).

Regarding MWs, except for 2012 when WIW was not observed, the four water masses were positively identified during all cruises. The lightest one is the WIW, which is at the top of the

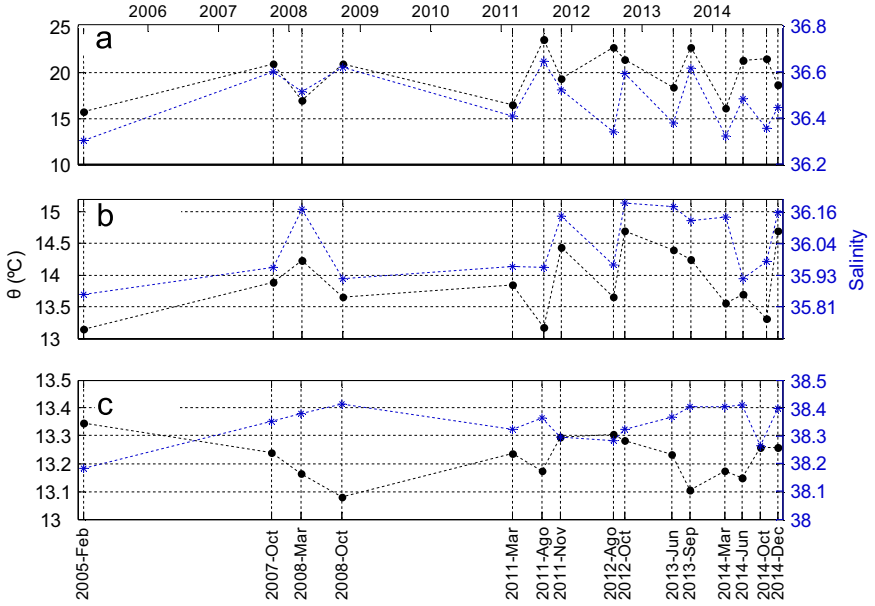

Fig. 9. Potential temperature (left axis, black points) and salinity (right axis, blue stars) of the water masses addressed in TES. Panel (a) is for SAW, panel (b) is for NACW, and panel (c) is for MW_{TES}. See text for details. Ticks in the *x*-axes at the top of the figure indicate January the 1st of each year. (For interpretation of the references to colour in this figure legend, the reader is referred to the web version of this article.)

Table 5
Mean values with standard deviation and trends of the potential temperature and salinity data displayed in Figure 8 and Figure 9. TES (shaded columns) correspond to the western exit of the Strait where MWs are not distinguishable and, therefore, a unique MW, denoted MW_{TES}, is specified (see text for details). Trend values in bold indicate that the trend is significant at the 95% significance level, while values in italics mean a non-significant trend at this level. Trends for NACW at TAC have not been computed since only four points were available.

	TES $\dot{\theta} \pm \sigma$ (°C)	**Trend** (°C/year)	**TAC** $\dot{\theta} \pm \sigma$ (°C)	**Trend** (°C/year)	**TES** $\dot{S} \pm \sigma$ (psu)	**Trend** (psu/year)	**TAC** $\dot{S} \pm \sigma$ (psu)	**Trend** (psu/year)
SAW	19.76 ± 2.60	*0.28*	19.74 ± 1.80	*0.18*	36.47 ± 0.12	*0.0047*	37.15 ± 0.08	*0.026*
NACW	13.91 ± 0.51	*0.05*	14.84 ± 0.14	-	36.03 ± 0.12	*0.017*	36.19 ± 0.07	-
WIW	-	-	13.11 ± 0.06	**0.030**	-	-	38.31 ± 0.07	**0.031**
MW_{TES}/LIW	13.22 ± 0.07	*0.0035*	13.20 ± 0.02	*-0.0064*	38.34 ± 0.06	*0.0087*	38.48 ± 0.01	*$9x10^{-4}$*
TDW	-	-	13.13 ± 0.03	*$9.3x10^{-4}$*	-	-	38.51 ± 0.005	*0.001*
WMDW	-	-	12.91 ± 0.02	**0.0089**	-	-	38.47 ± 0.07	**0.003**

Mediterranean layer between 150 and 260 m and it is detected in casts near the northern shore, in agreement with Fig. 7d. April 2014 was the exception as the WIW sample was detected deeper (293 m) and shifted to the south (cast 3), a situation that apparently extended until October 2014. LIW layer is beneath the WIW. Despite being spread out through the whole transect (Fig. 7d), its core is found in the northern part, usually at the position of cast number 5 (Fig. 8d) at depths between 260 and 300 m. April and October 2014 were again the exception, the LIW core was allways noticeably deeper. Curiously, warmer and fresher LIW was detected in 2012, coincidentally with the absence of WIW in the SoG. TDW is observed beneath the LIW between 370 and 550 m with preference to be detected close to the northern coast (casts 4 and 5), according to Fig. 8e. Once again April 2014 shows an anomalously large depth of the TDW core (567 m). Finally, the densest WMDW occupies the deepest layer with its core showing up close to the southern shore (casts 2 to 4) and always deeper than ~700 m except for November 2011, when it was detected at 566 m in cast number 2 (Fig. 8f). An absolute minimum of θ and S is observed in June 2009.

A similar analysis has been conducted at TES, taking into account only three water masses: SAW, NACW and what we shall refer to as MW_{TES}, a mixing of all the MWs that are no longer distinguishable. The representative sample of SAW and of NACW were the warmest and freshest ones, respectively, while MW_{TES} was represented by the saltiest sample. Fig. 9 displays the selected points for each cruise. As expected, seasonal fluctuations is the obvious characteristic of SAW (Fig. 9a), with warmer and also saltier water during the summer and early-autumn months. It is the most variable water mass, as can be deduced from Table 5 as well. The NACW (Fig. 9b) shows some seasonality, which consists in a diminution of θ in summer months. It would be associated with the upwelling-favourable winds in the Gulf of Cádiz, which uplift deeper and, hence, colder NACW, making it available for the inflow during the upwelling season (Folkard et al., 1997; Criado-Aldeanueva et al., 2006). A positive salinity trend is visible in Fig. 9b, only interrupted during the second part of 2014. The MW_{TES} (Fig. 9c) is the least variable water mass in this transect. Temperature and salinity display a rather specular pattern, suggesting that colder (warmer) water is simultaneously saltier (fresher), giving thus rise to enhanced fluctuations of density. MW_{TES} does not show a clear seasonality, neither a short-term trend, although from 2012 onwards the salinity is greater than the mean of the series (38.34, see Table 5).

5. Discussion and conclusions

The present study had the twofold objective of depicting the spatial distribution of the water masses participating in the exchange through the SoG and investigating the time variability of this pattern during the last years. An intensive oceanographic survey carried out in summer 2012 (GIC data) allowed us to address the first objective and the rather systematic CTD monitoring of two specific transects at both ends of the SoG (INGRES data) made it possible the analysis of the time variability.

5.1. Spatial variability

A cluster analysis was performed on GIC data to classify the water samples. Of all water masses reported in Table 1, the WIW was not detected and therefore it was excluded from the analysis. Also, after examining the five GIC transects and scrutinizing the zoomed θ–S diagrams of Fig. 3 and Fig. 4, it is questionable the inclusion of the TDW in the algorithm. If it is included the outcome of the analysis for the transects located east of CS provides a pattern with the LIW and TDW occupying preferably the northern part and the WMDW attached to the south (Figs. 3d and 4-I-II panel d). It is in good agreement with the previous study by Millot (2014b), who put forward that TDW flowing over the bottom piled up against the northern half of the SoG. Indeed, if we remove TDW from our analysis the samples which will correspond with TDW are divided between WMDW and LIW, with the samples incorporated to the LIW (WMDW) being located to the centre–north (centre–south) of the transect, without modifying heavily the distribution of Fig. 7 (not shown).

West of CS, the AWs are well differentiated but the MWs are not, according to the cluster analysis, which outputs LIW in all cases. This result is somewhat misleading as the proportion of all the MWs in the samples is very alike (Fig. 5). It is just because the proportion of LIW is slightly greater that the analysis ascribes the samples to the LIW cluster. Our interpretation, however, is that the intense tidal mixing undergone by the MWs flowing west over CS blurs out their specific characteristics, leaving a rather mixed water that we have denoted by MW_{TES}, whose characteristics depend on the tide to some extent. This would be the water making up the different veins of the Mediterranean outflow in studies dealing with the Gulf of Cadiz and Eastern North Atlantic Ocean circulation.

It should be remarked that there is not full consensus with this description. Millot (2014) put forward an organized structure of the Mediterranean outflow along the Iberian slope of the Gulf of Cadiz in four veins, each of them having its origin in one of the four MWs discussed so far. While our dataset does not allow for addressing this point in the Iberian slope west of the SoG, our observations in Espartel sill do not support such differentiation, especially regarding the vein supposedly ascribed to the WIW, which was absent during the GIC survey. The strong mixing reflected in the CTD transects west of Camarinal sill (Fig. 4b and 4c), which is further revealed by the cluster analysis (Fig. 4d), suggests that such a downstream organization of the Mediterranean veins is quite improbable at the time of the GIC survey, if not impossible.

Overall, the most significant result of the analysis of these data is the pronounced west-to-east erosion observed in the NACW, and of the MWs in the opposite way (Fig. 4b and 4c), which lose their specific identities. Both outcomes are a consequence of the outstanding mixing driven by tides that takes place in the Camarinal sill and its surroundings (Sánchez Garrido et al., 2011; Wesson and Gregg, 1994).

5.2. Temporal variability

The same cluster analysis has been performed on the whole set of INGRES data at TES and TAC transects (Fig. 7) with similar results. The main difference is the presence of WIW among the MWs in the eastern transect in 9 out of 11 cruises, which shows up embedded between the LIW and the AWs flowing close to the northern shore. Nevertheless, the goal of the INGRES data analysis is the investigation of the time variability, for which we have devised a criterion to identify the most representative samples of each of the water masses involved in the exchange during every cruise (Figs. 8 and 9). Mean values and trends during the period covered by the observations are summarized in Table 5. Mean values at the different transects merely inform about spatial variations and reflect the already discussed changes suffered by the NACW in its path to the MedS as well as the important mixing undertaken by the MWs after passing Camarinal sill. Interestingly the mean value of MW_{TES} potential temperature at the western transect (TES) is greater than any of the MWs mean values at the eastern transect (TAC), which implies that a small proportion of NACW must be involved in the MW_{TES} mixing. Salinity mean values also require the participation of NACW in the mixing (García Lafuente et al., 2007).

The marked seasonality of the SAW, and the NACW to some extent, along with the intermittent sampling of the transects make the trends reported in Table 5 to be very uncertain for the AWs (notice that trends for NACW are not computed at TAC due to the very small number of samples available). Apparently, NACW shows a tendency to increase its salinity from 2011 onwards at TES (Fig. 9b), although the drop by the summer of 2014 would deny this conclusion. Actually, the trend reported in Table 5 for this water is non-significant at the 95% confidence level. On the other hand, the fact that the seasonal expected drop of salinity during the previous summer (June 2013 cruise, Fig. 9b) had not taken place supports the salinity increase scenario, which otherwise would not be so apparent.

Trends in MWs are better investigated at the TAC transect. Six-year observations are obviously insufficient to speak of long-term trends, but some of the short-term trends that are drawn from our reduced dataset may be related to trends already mentioned in the literature (Borghini et al., 2014). During the studied period, neither the LIW nor the TDW show significant trends (Table 5), whereas both WIW and WMDW exhibit positive temperature and salinity trends, which are more pronounced for the former (Table 5). While the seasonality, intermittency, relatively small volume, and intermediate nature of the WIW formed in the northwest area of the Western MedS raise questions about the reaching and consequences of their estimated trends, the trends found for the WMDW will have more profound implications as they would be linked to similar trends in the interior of the MedS, which have been traced back up to several decades (Bethoux et al., 1990; Leaman and Schott, 1991; Rohling and Bryden, 1992; Krahmann and Schott, 1998). Recently, Borghini et al. (2014) have concluded that the MedS is becoming saltier, in which case the trend of WMDW in Table 5 would be nothing more than the mere reflection of this salinification. It is remarkable, however, that this trend is not observed in the MW_{TES} at TES section. A likely explanation would be that the WMDW is diluted with the rest of the MWs along the SoG, none of the later showing a significant trend, with the consequence that the WMDW trend at TAC fades out at TES.

The intermittency of WIW is illustrated in Fig. 8c. Traces of this water were not found either during the INGRES cruises carried out in August and November of 2012, or during the intensive GIC survey in July the same year (inset of Fig. 2). It suggests that WIW was not produced this year or, if so, the volume formed was quite small. Moored-based observations collected in the Gulf of Valencia near the area of WIW formation by Ribó et al. (2015) identify WIW passing by the mooring line in early spring of 2011, but not during late winter of 2012. Although the authors do not discard the possibility of WIW flowing above the moored instrumentation, the lack of WIW, or its fainter signal, in early 2012 would be connected with the absence of WIW in the SoG later on that year.

Almost coincidentally with this lack of WIW, the WMDW shows a relative potential temperature maximum in TAC (Fig. 8f) while MW_{TES} does the same at TES (Fig. 9c). It would be the reflection of a rather mild 2010–11 winter, as discussed in Severin et al (2014). Fig. 8f shows that the minimum WMDW potential temperature of all the period was reached in 2009, which could be related with the exceptional WMDW formation in the Gulf of Lion mentioned by (Salat et al., 2010). There are no data available at TES this year to support the observations at TAC transect, but it is noteworthy that similar strong events of WMDW formation left a recognizable footprint in the SoG.

Acknowledgement

This work is a Spanish contribution funded by the National Project INGRES 3 (CTM2010-21229), a French contribution to the HyMeX and MOOSE programmes funded by MISTRALS, and to the CIESM HYDROCHANGES Programme (ciesm.org/marine/programs/hydrochanges.htm). Cristina Naranjo acknowledges the fellowship BES-2011-043421 from the Ministry of Economy and Competitiveness – Spain, and M. Jesús Bellanco acknowledges the pre-doc fellowship IEO-FPI 2011/10. We are also grateful to the crews of the R/V Angeles Alvariño and the R/V TETHYS II, and to G. Rougier (MIO) and Deny Malengros (SAM/MIO) who operated the MVP. The MVP has been funded through the CETSM project.

Appendix A. Supplementary material

Supplementary data associated with this article can be found in the online version at http://dx.doi.org/10.1016/j.dsr.2015.08.003.

References

Baringer, M. 1993. Mixing and dynamics of the Mediterranean outflow (Ph.D. thesis).

Baringer, M.O.N., Price, J.F., 1997. Mixing and spreading of the mediterranean outflow. J. Phys. Oceanogr. 27 (8), 1654–1677. http://dx.doi.org/10.1175/1520-0485(1997)027 < 1654:MASOTM > 2.0.CO;2.

Ben Ismail, S., Schroeder, K., Sammari, C., Gasparini, G.P., Borghini, M., Aleya, L., 2014. Interannual variability of water mass properties in the Tunisia–Sicily channel. J. Mar. Syst. 135 (0), 14–28. http://dx.doi.org/10.1016/j.jmarsys.2013.06.010.

Bethoux, J.P., Gentili, B., Raunet, J., Tailliez, D., 1990. Warming trend in the western Mediterranean deep water. Nature 347 (6294), 660–662.

Borghini, M., Bryden, H., Schroeder, K., Sparnocchia, S., Vetrano, A., 2014. The Mediterranean is becoming saltier. Ocean Sci. 10 (4), 693–700. http://dx.doi.org/10.5194/os-10-693-2014.

Bray, N.A., Ochoa, J., Kinder, T.H., 1995. The role of the interface in exchange through the Strait of Gibraltar. J. Geophys. Res.: Oceans 100 (C6), 10755–10776. http://dx.doi.org/10.1029/95JC00381.

Bryden, H.L., Candela, J., Kinder, T.H., 1994. Exchange through the Strait of Gibraltar. Prog. Oceanogr. 33 (3), 201–248. http://dx.doi.org/10.1016/0079-6611(94)90028-0.

Bryden, H.L., Stommel, H.M., 1982. Origin of the Mediterranean outflow. J. Mar. Res. 40, 55–71.
Candela, J., Winant, C., Ruiz, A., 1990. Tides in the Strait of Gibraltar. J. Geophys. Res.: Oceans 95 (C5), 7313–7335. http://dx.doi.org/10.1029/JC095iC05p07313.
Conan, P., Millot, C., 1995. Variability of the northern current off marseilles, western mediterranean-sea, from february to june 1992. Oceanol. Acta 18 (2), 193–205.
Criado-Aldeanueva, F., García-Lafuente, J., Vargas, J.M., Del Río, J., Vázquez, A., Reul, A., Sánchez, A., 2006. Distribution and circulation of water masses in the Gulf of Cadiz from in situ observations. Deep Sea Res. Part II: Top. Stud. Oceanogr. *53* (11–13), 1144–1160. http://dx.doi.org/10.1016/j.dsr2.2006.04.012.
Folkard, A.M., Davies, P.A., Fiúza, A.F.G., Ambar, I., 1997. Remotely sensed sea surface thermal patterns in the Gulf of Cadiz and the Strait of Gibraltar: variability, correlations, and relationships with the surface wind field. J. Geophys. Res.: Oceans 102 (C3), 5669–5683. http://dx.doi.org/10.1029/96JC02505.
Font, J., 1987. The path of the Levantine intermediate water to the Alboran sea. Deep Sea Res. Part A. Oceanogr. Res. Papers 34 (10), 1745–1755. http://dx.doi.org/10.1016/0198-0149(87)90022-7.
Fuda, J.L., Millot, C., Taupier-Letage, I., Send, U., Bocognano, J.M., 2000. XBT monitoring of a meridian section across the western Mediterranean Sea. Deep Sea Res. Part I: Oceanogr. Res. Papers 47 (11), 2191–2218. http://dx.doi.org/10.1016/S0967-0637(00)00018-2.
García-Lafuente, J., Vargas, J.M., Plaza, F., Sarhan, T., Candela, J., Bascheck, B., 2000. Tide at the eastern section of the Strait of Gibraltar. J. Geophys. Res.: Oceans 105 (C6), 14197–14213. http://dx.doi.org/10.1029/2000JC900007.
García Lafuente, J., Bruque Pozas, E., Sánchez Garrido, J.C., Sannino, G., Sammartino, S., 2013. The interface mixing layer and the tidal dynamics at the eastern part of the Strait of Gibraltar. J. Mar. Syst. 117–118 (0), 31–42. http://dx.doi.org/10.1016/j.jmarsys.2013.02.014.
García Lafuente, J., Sánchez Román, A., Díaz del Río, G., Sannino, G., Sánchez Garrido, J.C., 2007. Recent observations of seasonal variability of the Mediterranean outflow in the Strait of Gibraltar. J. Geophys. Res.: Oceans 112 (C10), C10005. http://dx.doi.org/10.1029/2006JC003992.
García Lafuente, J., Sánchez Román, A., Naranjo, C., Sánchez Garrido, J.C., 2011. The very first transformation of the Mediterranean outflow in the Strait of Gibraltar. J. Geophys. Res.: Oceans 116 (C7), C07010. http://dx.doi.org/10.1029/2011JC006967.
Gascard, J.C., Richez, C., 1985. Water masses and circulation in the Western Alboran sea and in the Straits of Gibraltar. Prog. Oceanogr. 15 (3), 157–216. http://dx.doi.org/10.1016/0079-6611(85)90031-X.
Hur, H.B., Jacobs, G.A., Teague, W.J., 1999. Monthly variations of water masses in the Yellow and East China Seas, November 6, 1998. J. Oceanogr. 55 (2), 171–184. http://dx.doi.org/10.1023/A:1007885828278.
Kim, K., Kim, K.R., Rhee, T.S., Rho, H.K., Limeburner, R., Beardsley, R.C., 1991. Identification of water masses in the Yellow Sea and the East China Sea by cluster analysis. In: Takano, K. (Ed.), Elsevier Oceanography Series. Elsevier, Oxford, New York, pp. 253–267. http://dx.doi.org/10.1016/S0422-9894(08)70100-4.
Kinder, T.H., Bryden, H.L., 1990. Aspiration of deep waters through Straits. In: Pratt, L.J. (Ed.), The Physical Oceanography of Sea Straits. Springer, Netherlands, pp. 295–319. http://dx.doi.org/10.1007/978-94-009-0677-8_14.
Kinder, T.H., Parrilla, G., 1987. Yes, some of the Mediterranean outflow does come from great depth. J. Geophys. Res.: Oceans 92 (C3), 2901–2906. http://dx.doi.org/10.1029/JC092iC03p02901.
Krahmann, G., Schott, F., 1998. Longterm increases in western Mediterranean salinities and temperatures: Anthropogenic and climatic sources. Geophys. Res. Lett. 25 (22), 4209–4212. http://dx.doi.org/10.1029/1998GL900143.
Leaman, K.D., Schott, F.A., 1991. Hydrographic structure of the convection regime in the Gulf of Lions: winter 1987. J. Phys. Oceanogr. 21 (4), 575–598. http://dx.doi.org/10.1175/1520-0485(1991)021<0575:HSOTCR>2.0.CO;2.
Lopez Jurado, J.L., García Lafuente, J., Cano Lucaya, N., 1995. Hydrographic conditions of the Ibiza channel during November 1990, March 1991 and July 1992. Oceanol. Acta 18 (2), 235–243 (doi:http://archimer.ifremer.fr/doc/00097/20868/).
Millot, C., 1999. Circulation in the Western Mediterranean Sea. J. Mar. Syst. 20 (1–4), 423–442. http://dx.doi.org/10.1016/S0924-7963(98)00078-5.
Millot, C., 2009. Another description of the Mediterranean Sea outflow. Prog. Oceanogr. 82 (2), 101–124. http://dx.doi.org/10.1016/j.pocean.2009.04.016.
Millot, C., 2014a. Heterogeneities of in- and out-flows in the Mediterranean Sea. Prog. Oceanogr. 120 (0), 254–278. http://dx.doi.org/10.1016/j.pocean.2013.09.007.
Millot, C., 2014b. Levantine Intermediate Water characteristics: an astounding general misunderstanding!. Sci. Mar. 78 (2), 165–171. http://dx.doi.org/10.3989/scimar.04045.30H.
Millot, C., Candela, J., Fuda, J.-L., Tber, Y., 2006. Large warming and salinification of the Mediterranean outflow due to changes in its composition. Deep Sea Res. Part I: Oceanogr. Res. Papers 53 (4), 656–666. http://dx.doi.org/10.1016/j.dsr.2005.12.017.
Millot, C., Taupier-Letage, I., 2005. Circulation in the Mediterranean Sea. In: Saliot, A. (Ed.), The Mediterranean Sea. Springer, Berlin, Heidelberg, pp. 29–66. http://dx.doi.org/10.1007/b107143.
Monserrat, S., López-Jurado, J.L., Marcos, M., 2008. A mesoscale index to describe the regional circulation around the Balearic Islands. J. Mar. Syst. 71 (3–4), 413–420. http://dx.doi.org/10.1016/j.jmarsys.2006.11.012.
Naranjo, C., García-Lafuente, J., Sánchez-Garrido, J.C., Sánchez-Román, A., Delgado-Cabello, J., 2012. The Western Alboran Gyre helps ventilate the Western Mediterranean Deep Water through Gibraltar. Deep Sea Res. Part I: Oceanogr. Res. Papers 63 (0), 157–163. http://dx.doi.org/10.1016/j.dsr.2011.10.003.
Naranjo, C., Garcia-Lafuente, J., Sannino, G., Sanchez-Garrido, J.C., 2014. How much do tides affect the circulation of the Mediterranean Sea? From local processes in the Strait of Gibraltar to basin-scale effects. Prog. Oceanogr. 63 (0). http://dx.doi.org/10.1016/j.pocean.2014.06.005.
Parrilla, G., Kinder, T.H., 1987. The Physical Oceanography of the Alboran Sea Rep. DTIC Document.
Parrilla, G., Kinder, T.H., Preller, R.H., 1986. Deep and intermediate mediterranean water in the western Alboran Sea. Deep Sea Res. Part A. Oceanog. Res. Papers 33 (1), 55–88. http://dx.doi.org/10.1016/0198-0149(86)90108-1.
Pettigrew, N.R., 1989. Direct measurements of the flow of western Mediterranean deep water over the Gibraltar sill. J. Geophys. Res.: Oceans 94 (C12), 18089–18093. http://dx.doi.org/10.1029/JC094iC12p18089.
Pinot, J.M., López-Jurado, J.L., Riera, M., 2002. The CANALES experiment (1996–1998). Interannual, seasonal, and mesoscale variability of the circulation in the Balearic Channels. Prog. Oceanogr. 55 (3–4), 335–370. http://dx.doi.org/10.1016/S0079-6611(02)00139-8.
Rhein, M., Send, U., Klein, B., Krahmann, G., 1999. Interbasin deep water exchange in the western Mediterranean. J. Geophys. Res.-Oceans 104, 23495–23508. http://dx.doi.org/10.1029/1999jc900162.
Ribó, M., Puig, P., van Haren, H., 2015. Hydrodynamics over the Gulf of Valencia continental slope and their role in sediment transport. Deep Sea Res. Part I: Oceanogr. Res. Papers 95 (0), 54–66. http://dx.doi.org/10.1016/j.dsr.2014.10.004.
Rohling, E.J., Bryden, H.L., 1992. Man-induced salinity and temperature increases in western Mediterranean deep water. J. Geophys. Res.: Oceans 97 (C7), 11191–11198. http://dx.doi.org/10.1029/92JC00767.
Salat, J., Font, J., 1987. Water mass structure near and offshore the Catalan coast during the winters of 1982 and 1983. Ann. Geophys. Ser. B 5 (1), 49–54.
Salat, J., Puig, P., Latasa, M., 2010. Violent storms within the sea: dense water formation episodes in the NW Mediterranean. Adv. Geosci. 26, 53–59. http://dx.doi.org/10.5194/adgeo-26-53-2010.
Sánchez Garrido, J.C., García Lafuente, J., Criado Aldeanueva, F., Baquerizo, A., Sannino, G., 2008. Time–spatial variability observed in velocity of propagation of the internal bore in the Strait of Gibraltar. J. Geophys. Res.: Oceans 113 (C7). http://dx.doi.org/10.1029/2007JC004624, n/a-n/a.
Sánchez Garrido, J.C., Sannino, G., Liberti, L., García Lafuente, J., Pratt, L., 2011. Numerical modeling of three-dimensional stratified tidal flow over Camarinal Sill, Strait of Gibraltar. J. Geophys. Res.: Oceans 116 (C12), C12026. http://dx.doi.org/10.1029/2011JC007093.
Sánchez Román, A., Criado Aldeanueva, F., García Lafuente, J., Sánchez Garrido, J.C., 2008. Vertical structure of tidal currents over Espartel and Camarinal sills, Strait of Gibraltar. J. Mar. Syst. 74 (1–2), 120–133. http://dx.doi.org/10.1029/2011JC007093.
Sánchez Román, A., García Lafuente, J., Delgado, J., Sánchez Garrido, J.C., Naranjo, C., 2012. Spatial and temporal variability of tidal flow in the Strait of Gibraltar. J. Mar. Syst. 98–99 (0), 9–17. http://dx.doi.org/10.1016/j.jmarsys.2012.02.011.
Santinelli, C., Ribotti, A., Sorgente, R., Gasparini, G.P., Nannicini, L., Vignudelli, S., Seritti, A., 2008. Coastal dynamics and dissolved organic carbon in the western Sardinian shelf (Western Mediterranean). J. Mar. Syst. 74 (1–2), 167–188. http://dx.doi.org/10.1016/j.jmarsys.2007.12.005.
Severin, T., Conan, P., Durrieu de Madron, X., Houpert, L., Oliver, M.J., Oriol, L., Caparros, J., Ghiglione, J.F., Pujo-Pay, M., 2014. Impact of open-ocean convection on nutrients, phytoplankton biomass and activity. Deep Sea Res. Part I: Oceanogr. Res. Papers 94 (0), 62–71. http://dx.doi.org/10.1016/j.dsr.2014.07.015.
Smith, R.O., Bryden, H.L., Stansfield, K., 2008. Observations of new western Mediterranean deep water formation using Argo floats 2004–2006. Ocean Sci. 4 (2), 133–149. http://dx.doi.org/10.5194/os-4-133-2008.
Stommel, H., Bryden, H., Mangelsdorf, P., 1973. Does some of the Mediterranean outflow come from great depth? Pageoph. 105 (1), 879–889, http://dx.doi.org/10.1007/BF008758837..
Vargas-Yáñez, M., Plaza, F., García-Lafuente, J., Sarhan, T., Vargas, J.M., Vélez-Belchi, P., 2002. About the seasonal variability of the Alboran Sea circulation. J. Mar. Syst. 35 (3–4), 229–248. http://dx.doi.org/10.1016/S0924-7963(02)00128-8.
Vargas-Yáñez, M., Zunino, P., Schroeder, K., López-Jurado, J.L., Plaza, F., Serra, M., Castro, C., García-Martínez, M.C., Moya, F., Salat, J., 2012. Extreme Western Intermediate Water formation in winter 2010. J. Mar. Syst. 105–108 (0), 52–59. http://dx.doi.org/10.1016/j.jmarsys.2012.05.010.
Warn-Varnas, A., Gangopadhyay, A., Hawkins, J.A., Robinson, A.R., 2005. Wilkinson Basin area water masses: a revisit with EOFs. Cont. Shelf Res. 25 (2), 277–296. http://dx.doi.org/10.1016/j.csr.2004.09.005.
Wesson, J.C., Gregg, M.C., 1994. Mixing at Camarinal Sill in the Strait of Gibraltar. J. Geophys. Res.: Oceans 99 (C5), 9847–9878. http://dx.doi.org/10.1029/94JC00256.
Whitehead, J.A., 1985. A laboratory study of gyres and uplift near the Strait of Gibraltar. J. Geophys. Res.: Oceans 90 (C4), 7045–7060. http://dx.doi.org/10.1029/JC090iC04p07045.
Yan, M., 2005. Methods of Determining the Number of Clusters in a Data Set and a New Clustering Criterion, Virginia, Blacksburg.